Ray-Optical Prediction of Radio-Wave Propagation Characteristics in Tunnel Environments—Part 2: Analysis and Measurements

Y. P. Zhang, Y. Hwang, and R. G. Kouyoumjian

***Abstract*—The uniform theory of diffraction (UTD) developed in Part 1 is used to predict narrow- and wide-band propagation characteristics in tunnels at 900- and 1800-MHz frequencies. Narrow-band propagation characteristics is shown in spatial domain and wide-band propagation in time domain. In empty straight-tunnel environments, propagation exhibits a break-point phenomenon and has very short time delay spread. In empty curved or branched tunnel environments, propagation suffers higher loss. Vehicles cause additional propagation loss and larger varying time delay spread in tunnels. The measured results have validated the accuracy of the theoretical model and provided important information on narrow-band and wide-band propagation characteristics in empty, branched and obstructed tunnels.**

I. Introduction

MOBILE and personal communications services aim to provide users excellent communications without time and space constraints. Constructing such versatile networks relies heavily on the microcellular scheme, thus minimizing the cell size in order to increase frequency reuse and facilitating a much higher system capacity. The development of optimally designed microcells requires thorough radio-wave propagation characteristics; therefore, both theoretical and experimental propagation studies have been extensively undertaken [1]. For instance, measurements made in rural areas showed that the rural propagation mechanism was due to direct and ground-reflected waves [2]. Suburban propagation measurements were more random in nature, possibly due to the presence of more than one reflected ray [3], [4]. Studies related to urban propagation mechanisms have received much attention since the vast majority of communications takes place in the metropolis [5]–[7]. Recently, propagation research has begun to concentrate on the characterization of radio channels in indoor environments such as in houses, office buildings, and factories [8]–[10]. In this paper, the propagation of UHF radio wave in tunnels is studied by both theoretical model and measurements.

The tunnels constitute special radio propagation environments and have strong guiding propagation characteristics. If the radio signal frequency is lower than the tunnel cutoff frequency, propagation will suffer considerable attenuation. On the other hand, if the radio-signal frequency is much higher than the tunnel cutoff frequency, propagation will attenuate less than that in free-space [11], [12]. A theoretical model based on the modal theory has been proposed to explain tunnel guiding propagation characteristics [13]–[15]. This model treats a tunnel as a hollow oversized imperfect waveguide. Propagation is governed by a fundamental mode and an infinite number of higher order modes. The model is complicated because the coupling of these modes arises due to the imperfection of the waveguide. Another theoretical model based on the geometrical optic theory was then proposed [16]. The geometrical optic theory considers the tunnel walls as reflected planes. Propagation is achieved via a direct path and all possible reflected paths. Both theories are restricted to empty straight tunnels and, thus, have limitations. A more comprehensive model that can better approximate the actual tunnel environments is needed.

Our developed diffraction was utilized in the propagation model. The walls of tunnels were approximated by uniform surface impedance. The implementation of our tunnel uniform theory of diffraction (UTD) propagation model is described in Section II. Calculated and measured narrow-band results at 900 and 1800 MHz in empty, branched, and obstructed tunnels are compared in Section III and those for wide-band in Section IV. Our comparisons demonstrate that this propagation model is capable of simulating basic tunnel propagation characteristics with excellent accuracy. Section V summarizes the results.

II. Tunnel Propagation Model

The geometry of a typical tunnel complex is shown in Fig. 1. A transmit antenna T_x is located in the main tunnel of width A and height B meters. The branch tunnel has width C meters at a distance Z_b meters from the transmitter. A rectangular metallic box of width V_a, height V_b, and length V_l meters represents a vehicle with its rear lower corner located at a distance x_v meters from the left wall and at a distance z_v meters from the transmitter of the main tunnel. The tunnel walls are assumed to be a lossy nonmagnetic homogeneous medium with relative permittivity ε_r and conductivity σ. The transmit antenna T_x is positioned h_r meters above the floor and x_t meters from the left wall. A receive antenna R_x is placed

Manuscript received May 23, 1995; revised February 15, 1997. This work was supported in part by the National Natural Science Foundation of China.

Y. P. Zhang is with Nanyang Technological University, School of Electrical and Electronic Engineering, Singapore 639798, on leave from Taiyuan University of Science and Technology, Shanxi, R.O.C..

Y. Hwang is with Pinnacle EMwave, CA 94022 USA.

R. G. Kouyoumjian is with the Department of Electrical Engineering, The Ohio State University, Columbus, OH 43212 USA.

Publisher Item Identifier S 0018-926X(98)07058-6.

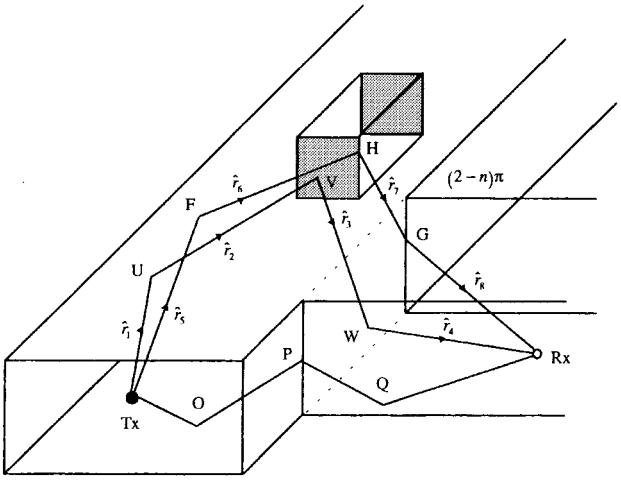

Fig. 1. Geometry of the propagation model.

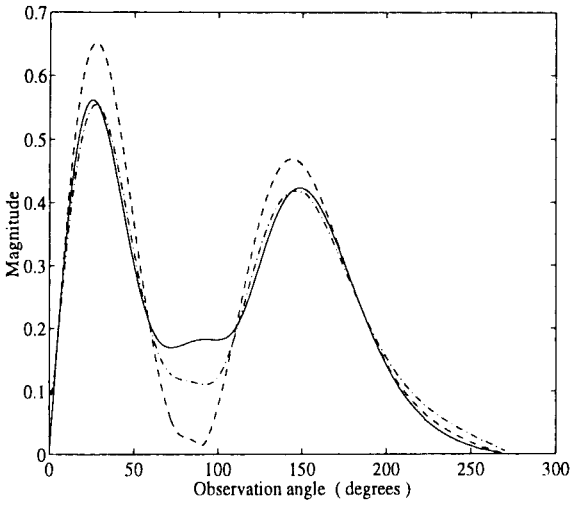

Fig. 2. Patterns of the total horizontally polarized field for a point source in the presence of a right-angle wedge with equal face impedance.

h_t meters above the floor and its position is moved either in the main or branch tunnels. Fig. 1 shows three major rays, T_x UVW R_x, T_x OPQ R_x, T_x FHG R_x, reaching the receiver in the branch tunnel for a source located in the main tunnel and far away from the corner. Path T_x UVW R_x represents the ray with multiple reflections, path T_x OPQ R_x, the ray with multiple reflections and single diffraction from a wedge, and path T_x FHG R_x, a ray with multiple reflections and double diffractions from any two successive significant wedges. Such are the three dominant propagation rays to be considered in this tunnel propagation model.

The received power is mathematically expressed in general as

$$P_r \approx \left(\frac{\lambda}{4\pi}\right)^2 P_t \Bigg| \sum_i \left(\prod_{k_r} R_{ik_r}\right) \times G_{ti} G_{ri} S_i \Phi_i + \sum_u \sum_w \left(\prod_{k_{rb}} R_{uk_{rb}}\right) \times D_{wu} \left(\prod_{k_{ra}} R_{uk_{ra}}\right) G_{tu} G_{ru} S_u \Phi_u + \sum_v \sum_q \left(\prod_{k_{rc}} R_{vk_{rc}}\right) D_{wv} D_{w+1v} \times \left(\prod_{k_{rd}} R_{vk_{rd}}\right) G_{tv} G_{rv} S_v \Phi_v \Bigg|^2. \quad (1)$$

In (1), the first term represents the contribution to the received signal power from such rays grouped by i having undergone k_r times reflection but with no diffraction from any wedge. The second term accounts for the contribution to the received signal power from the rays labeled by u having undergone k_{rb} times reflection before a single diffraction from wedge w occurs and subsequently undergone reflection k_{ra} times. The third term denotes the contribution to the received signal power from the vth rays having undergone k_{rc} times reflection before double diffraction from any two successive significant wedges occurs and subsequently undergone reflection k_{rd} times. k_r, k_{ra}, k_{rb}, k_{rc}, and k_{rd} in (1) will depend on the values of relative permittivity ε_r and conductivity σ of the tunnel walls, and the geometry of the tunnel. Each term in (1) is explained in detail in the Appendix.

The diffraction coefficients in (1) were given in Part 1. Other forms of diffraction coefficients that have been widely used are given in [17]. In order to show the difference between the two forms of diffraction coefficients, a radiation pattern for a point source at $(S' = 10\lambda, \phi' = 30°)$ in the presence of a right-angle impedance wedge with equal face impedance ($\varepsilon_r = 10, \sigma = 0.01$ s/m) is computed and presented in Fig. 2. The continuous line is calculated from the new rigorous diffraction coefficients, whereas the dashed-dot line is from the widely used diffraction coefficients given in [17]. The result for a perfectly conducting wedge is plotted by dashed line to illustrate the effect of the impedance boundary conditions. Our diffraction coefficients show a lower fluctuation of the total field.

The computer program is written in a modular fashion. The program uses the technique of ray tracing to identify ray paths intercepted by the receive antenna. The code first analyzes the input geometry in the geometry subroutine. The tunnel is described by finite number of surfaces and edges that are expressed in plane and straight line equations in a prescribed order. The locations of both the transmit and receive antennas are defined. It also gives an *a priori* indication of the regions where different terms need to be included. The ray tracing is accomplished by a complete search of a ray tree, accounting for the decomposition of the ray at each intersection. Having checked the direct path, the program traces a ray from the transmit antenna in a predetermined direction to search for an intersection. If an intersection has occurred, it first determines whether it is a reflection or diffraction, followed by a checking of whether the ray can directly reach the receiver or not. Otherwise, it will continue to trace the reflected or diffracted ray into subsequent reflection and diffraction until a maximum number of tree levels is reached or when the ray energy is negligible. The code finally checks if this reflected or diffracted ray reaches the reception sphere of the receive antenna. The

reception sphere has a radius of $L\alpha/\sqrt{3}$ [9], where L is the total path length of the ray from the transmit antenna to the receive antenna, α is the constant angular spacing between neighboring rays at the transmit antenna. If this ray intersects the sphere, it also intersects the receiver. Otherwise, the ray is not received. The simulated results were obtained by tracing rays to four levels with $\alpha = 5°$. Once a complete ray path is identified, the receive field is first computed in the local ray-coordinated system and then transformed into a reference-coordinated system.

Even though the tunnel propagation model is developed for a rectangular tunnel, it can also be extended to predict propagation in an arched tunnel using the principle of equivalence. The propagation was shown to be insensitive to the shape of cross section [15]. The arched tunnel can be treated as an equivalent rectangular tunnel. The equivalent width is set to be equal to the width of the original arched tunnel, while the height can thus be obtained by assuming that the equivalent tunnel has the same cross section as the original arched tunnel.

The tunnel propagation model provides information about the tunnel wide-band channel characteristics that are quantified by the rms delay spread $\tau_{\rm rms}$ defined below:

$$\tau_{\rm rms} = \sqrt{\frac{\sum_x P_{rx}\tau_x^2}{\sum_x P_{rx}} - \bar{\tau}^2} \tag{2}$$

where $\bar{\tau} = \frac{\sum_x P_{rx}\tau_x}{\sum_x P_{rx}}$ is the mean excess time delay and P_{rx} is the received power from the xth ray. The delay spread $\tau_{\rm rms}$ gives an indication of the potential for the intersymbol interference in digital transmission. Measurements have been conducted in various actual tunnel environments [18]. These measured data were used to assess the validity of the propagation model.

III. Narrow-Band Comparison with Measurements

Narrow-band characterization of radio wave propagation channels concerns both local and global variations of received signal levels. The narrow-band comparison was made in spatial domain on a relative basis.

A. Narrow-Band Propagation in Empty Straight Tunnels

The first comparison illustrated in Fig. 3 was made in an empty straight road tunnel. It is 2000 m long with a rectangular cross section 4 m high and 7.5 m wide. Curve (1) shows the measured result of the variation of the received signal power level versus the distance between the transmitter and the receiver at 900 MHz. The transmit and receive antennas are half-wavelength dipoles, vertically polarized and located at and $(0.25A, 0.3B, Z_0)$ and $(0.2A, 0.3B, Z)$, respectively. Curve (2) represents the simulated received power from the propagation model, which has been vertically displaced from curve (1) for better comparison. The longitudinal spatial patterns of the simulated and measured results are quite similar.

The second comparison was made in the empty straight section of a coal mine haulageway tunnel with an arched cross section maximum 3.0 m high and 4.2 m wide. Curves

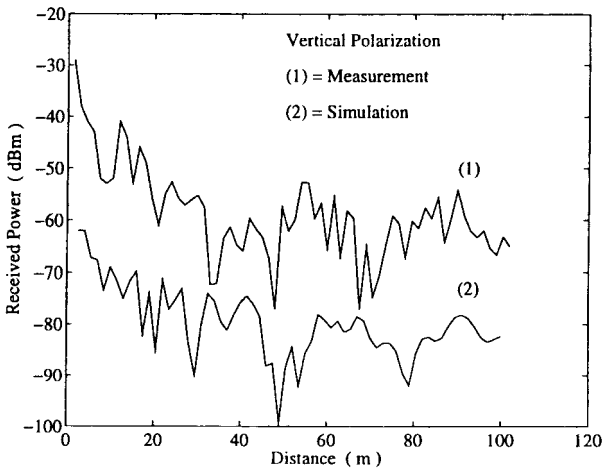

Fig. 3. Measured and simulated received power at 900 MHz in a straight empty rectangular road tunnel (the simulated one is displaced 30 dB downward).

(1) in Fig. 4(a) and (b) illustrates the measured results of the variations of the received signal power levels versus the distance between the transmitter and the receiver at 900 MHz for horizontal and vertical polarization, respectively. Curves (2) in Fig. 4(a) and (b) represents the calculated results from its equivalent 4.2-m-wide and 2.9-m-high rectangular tunnel obtained according to the criteria stated previously. Again, the simulated propagation results agree well with the measured values. Fig. 4(a) and (b) clearly shows that important fluctuations of the received signals appear in the vicinity of the transmit antenna, irrespective of polarization. In the short distance region, more significant reflected rays cause large fluctuations, whereas in the long distance region as the reflected rays become less significant, the direct ray contributes the most to the received signal. Therefore, the magnitude of fluctuations diminishes as the receiver moves further away from the transmitter. Both measurements and predictions show the existence of a distinct break point along the line-of-sight path, before and after which the propagation has different rate of attenuation. This propagation behavior was observed in other radio environments as well. The method of determining the location of the break point was given in [19], which can estimate the position of the break point in tunnel environments. Not having taken this break point into consideration, the existing tunnel waveguide model has overestimated the coverage distance.

B. Narrow-Band Propagation in Branched Tunnels

Fig. 5(a) and (b) illustrates the additional loss in the tunnel branch to the power of the received signals of both horizontal and vertical polarization, respectively. Curves (1) represent the measured results from a tunnel complex of 4.2 m wide and 3.0 m high. During the experiment, the transmitter positioned in the middle of the branch tunnel was 10 m away from the junction formed by the branch and the main tunnel at an angle of 15°. As the receiver was being moved from the branch tunnel into the main one, the received signal power initially dropped rapidly and leveled off in the junction vicinity. Curves

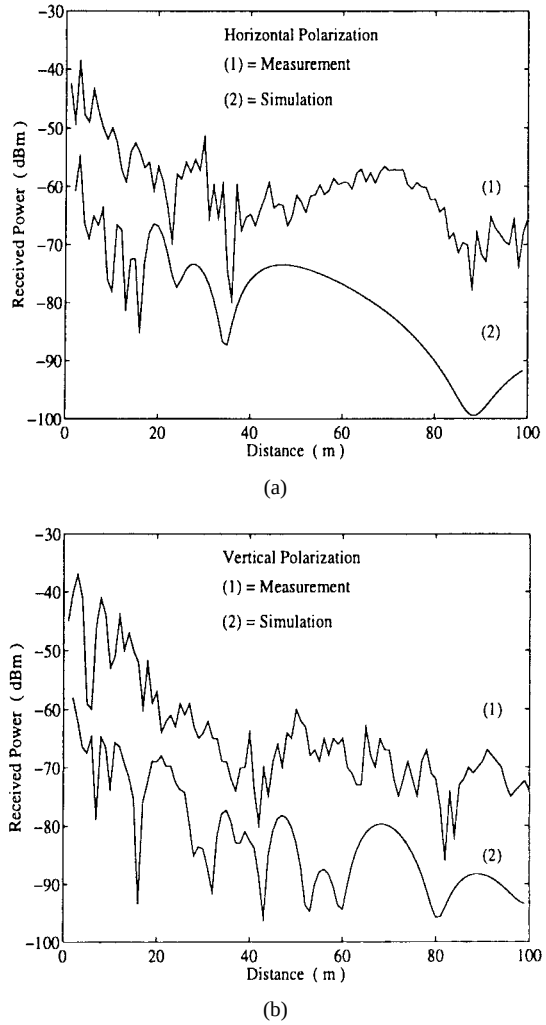

Fig. 4. Measured and simulated received power at 900 MHz in a straight empty arched coal mine haulageway tunnel (the simulated is displaced 20 dB downward).

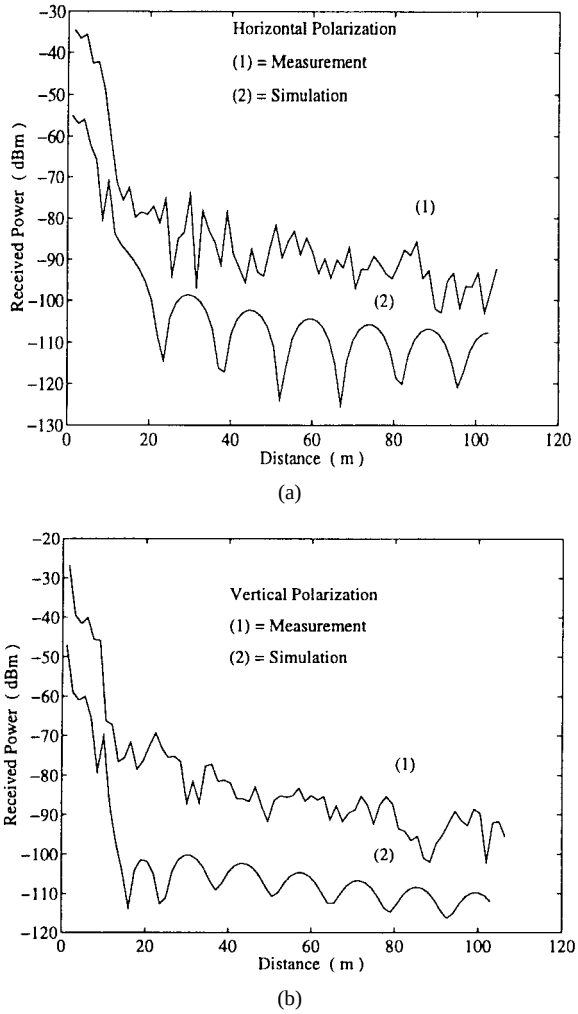

Fig. 5. Measured and simulated received power at 900 MHz in a branched empty arched coal mine haulageway tunnel (the simulated is displaced 20 dB downward).

(2) are the calculated results from our tunnel propagation model with the electrical characteristics of the tunnel walls being $\sigma = 10^{-2}$ s/m and $\varepsilon_r = 10$. Again, the simulated and measured propagation patterns mirror each other with small peaks and dips. These peaks and dips, which were also observed in urban radio propagation environments [5] were caused by scattering of small objects in the vicinity of the receiver. The computer simulation showed that the first term in (1) dominated at the junction, the second term in the region far away from the junction, and the third term was insignificant.

C. Narrow-Band Propagation in Obstructed Tunnels

Fig. 6(a) shows 900-MHz vertically polarized radio wave propagation in a two-lane tunnel blocked by a truck 64 m away from the tunnel entrance. Curve (1) represents the measured received signal power from [20]. Curve (2) is the calculated result from our tunnel propagation model with the electrical characteristics of the tunnel walls of $\sigma = 10^{-2}$ s/m and $\varepsilon_r = 5$. There is a good agreement between the measured and simulated results. Fig. 6(b) compares the 900-MHz simulated undisturbed propagation result against the pattern caused by the truck in the tunnel. The presence of the truck produces two undesirable effects: 1) making the received signal power exhibit more severe fluctuations and 2) resulting in additional loss behind the truck. In this case the third term of 1) could no longer be neglected and became the dominant one, particularly behind the truck.

The narrow-band comparison has shown the best agreement between simulated and measured received signal power for empty straight tunnels. The average error and standard deviation are 1.9 and 2.7 dB in empty straight tunnels, 2.37 and 3.86 dB in empty branched tunnels and 2.2 and 4.1 dB in obstructed tunnels.

IV. Wide-Band Comparison with Measurements

The wide-band comparison was made in temporal domain. Information concerning wide-band signal propagation in tunnel environments was not available until we performed wide-band propagation measurements in the Hong Kong NS 173 tunnel by using the swept frequency technique [18]. The rectangular concrete subway tunnel under test is 3.43 m wide, 2.6 m high, and 258.7 m long. In our measurements, the

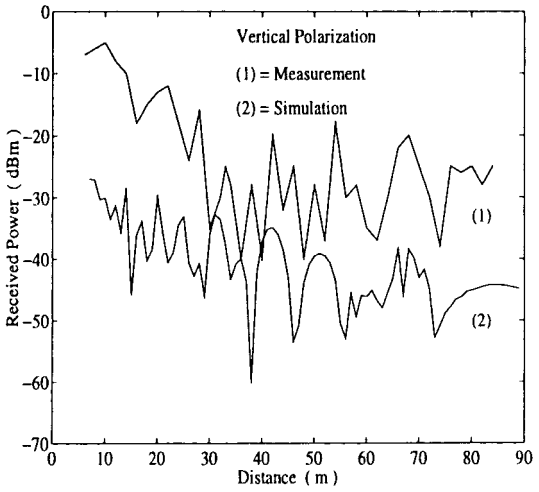

(a)

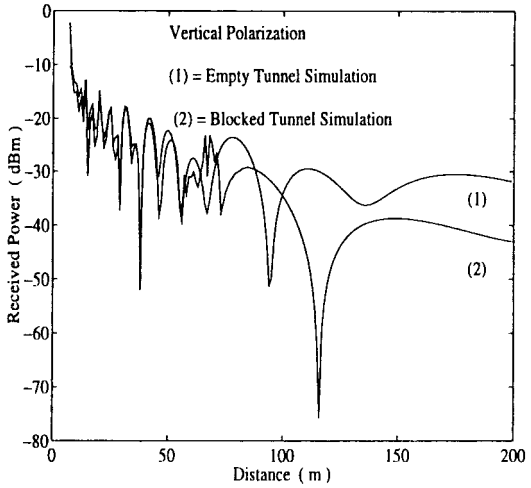

(b)

Fig. 6. Measured and simulated received power at 900 MHz in a vehicle-blocked tunnel (the simulation is displaced 20 dB downward).

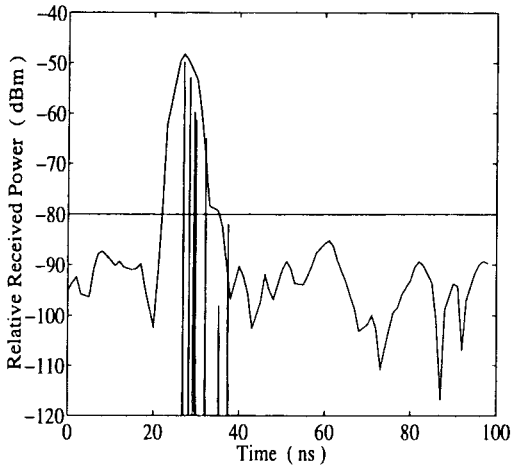

(a)

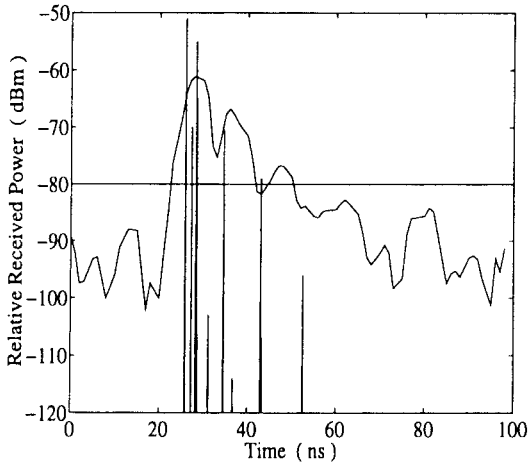

(b)

Fig. 7. Measured and simulated power-delay profiles at 900 and 1800 MHz in a straight and empty tunnel.

tunnel wide-band radio propagation channels were excited over 400-MHz band at the central frequencies of 900 and 1800 MHz. The distortion of each frequency component caused by the tunnel environment was measured. The temporal domain characteristics were then obtained from the inverse Fourier transformation of the measured frequency domain data. The power-delay profiles were given on a scale of 2.5-ns resolution and a 1.0-μs repetitive period. Rappaport *et al.* [21] developed an empirical and analytical technique to interpret the measured wide-band data. They discussed the measurement system and the selection of the threshold level such as the importance of using the measurement system with sensitivity comparable to commercial radiophones. The noise floor of 104 dBm for the 4-MHz bandwidth measurement system corresponded to the noise floor of -125 dBm for commercial 30-kHz bandwidth cellular phones. Thus, for our 400-MHz bandwidth measurement system, the corresponding noise floor should be -84 dBm, which would yield a threshold of -74 dBm for an input 10-dB SNR. Our threshold is between -74 and -80 dBm. They are represented by a horizontal line in Figs. 7–11.

A. Wide-Band Propagation in an Empty Straight Tunnel

Fig. 7(a) and (b) shows measured and simulated 900-MHz horizontally and 1800-MHz vertically polarized power-delay profiles for the straight section of the tunnel by locating the transmit and receive disc-cone antennas at $(0.5A, 0.5B, 0.0)$ and $(0.5A, 0.5B, 5)$, respectively. There are more simulated pulses than the measured ones above the threshold level. This might be expected as the simulation has much higher resolution than the measurement. For the 900-MHz horizontally polarized power delay profiles, there are five simulated pulses versus two measured pulses. The maximum arrival time difference among the first four waves is 2.5 ns, which is the resolution limit of the measurement system. As a result, they merged to the first measured pulse. The fifth simulated pulse has a longer delay and is the second measured pulse. The measured and simulated root mean square (rms) delay spreads are 2.4 and 2.42 ns, respectively. For the 1800-MHz vertically polarized power delay profiles, there are three measured pulses above the threshold level. The simulated power delay profile predicts the amplitudes and arrival times of the significant multipath components. Great similarity is exhibited in the rms delay, with the higher frequency signal having a longer delay spread.

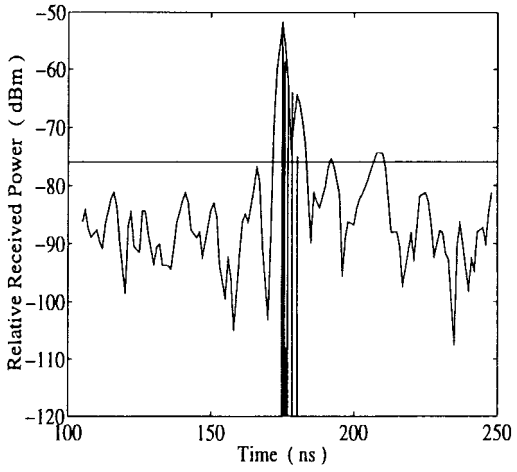

(a)

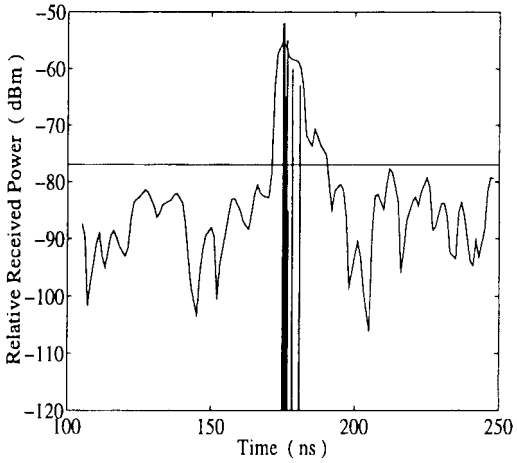

(b)

Fig. 8. Measured and simulated power-delay profiles at 900 MHz for horizontal and vertical polarization in a straight and empty tunnel.

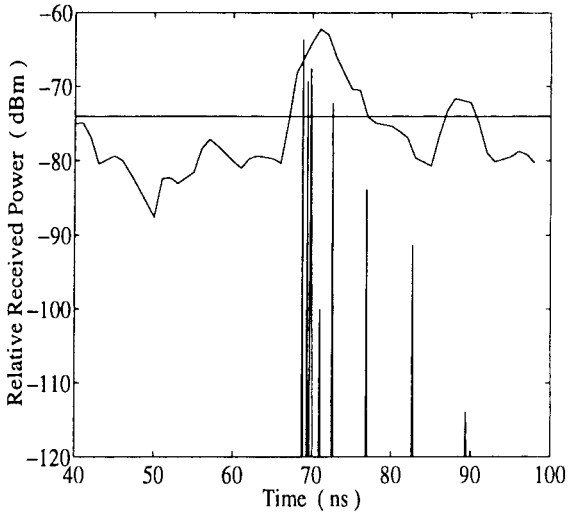

Fig. 9. Measured and simulated vertical polarized power-delay profiles at 900 MHz with the transmit antenna outside the tunnel and the receive antenna inside.

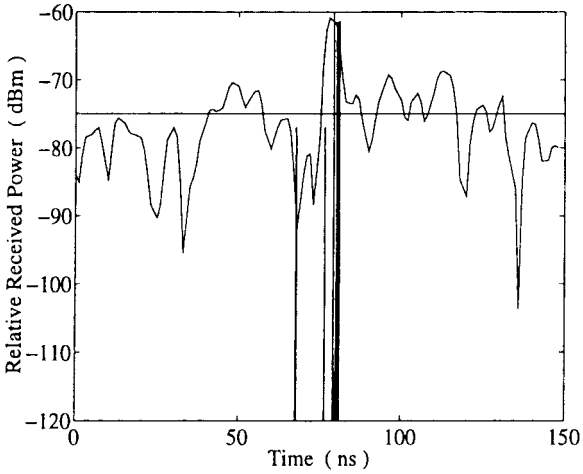

Fig. 10. Measured and simulated vertically polarized power-delay profiles at 900 MHz in an obstructed tunnel.

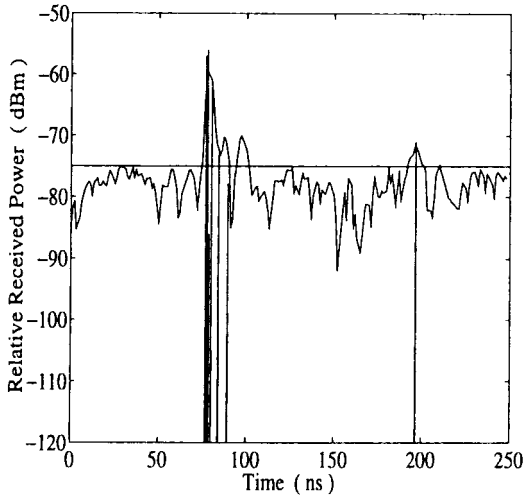

(a)

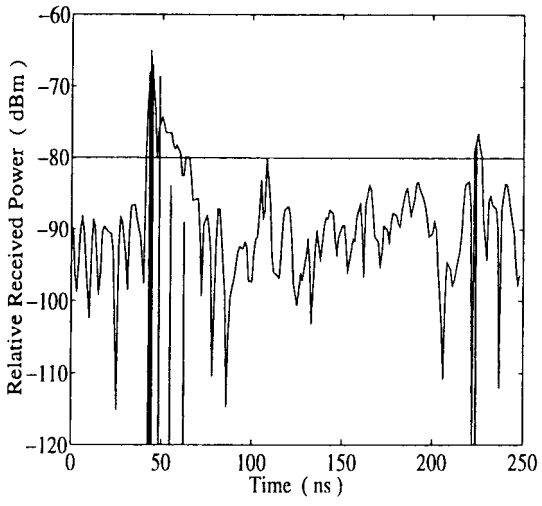

(b)

Fig. 11. Measured and simulated vertically polarized power-delay profiles at 900 and 1800 MHz in a straight tunnel with a vehicle.

Fig. 8(a) and (b) displays the 900-MHz measured versus simulated power-delay profiles for horizontal and vertical polarization with 50-m separation between the transmit and receive antennas. The amplitudes and arrival times of direct path and shorter delay multipath components are correctly predicated. However, the multipath components with longer

delay were not traced due to the existence of a more complex propagation environment in the more distant experiment locations. The horizontally polarized power-delay profiles spread somewhat wider than the vertically polarized ones. For instance, the measured and simulated rms delay spreads for the profiles shown were 13.5 and 10.1 ns for horizontal polarization and were decreased to 5.49 and 6.2 ns, respectively, for vertical polarization. The different rms delay spreads are caused by different attenuation constants for the two polarizations. The smaller attenuation of the horizontally polarized waves makes the power-delay profile spread wider.

The propagation is crucial near both the tunnel entrance and the exit. A theoretical approach based on the UTD has been proposed to predict narrow-band propagation in transition regions [22]. Fig. 9 presents the measured 900-MHz vertically polarized power-delay profile with the transmit antenna outside and the receive antenna inside the tunnel. The simulated results were also included for comparison. The amplitudes and arrival times of major multipath components could be clearly identified. The amplitude of the first measured pulse became smaller compared with that in Fig. 8(b), although the line-of-sight propagation path maintained and the distance between the transmit and receive antennas was only 30 m long. This clearly indicates the difficulty of guiding the power to and from the tunnel.

B. Wide-Band Propagation in an Obstructed Tunnel

Comparison of the measured and simulated power delay profiles were also conducted in more complex measurement locations. Fig. 10 illustrates the measured 900-MHz vertically polarized power-delay profile obtained from a vehicle in an obstructed location compared to the simulated result. Since the higher order diffracted rays were not included, the predicted profile did not contain as many multipath components as were measured. The predicted rms delay spread was different from the measured one. Higher order diffracted rays are generally difficult to implement in the analysis and present a practical limitation in the application of the geometrical theory of diffraction.

Fig. 11(a) shows the 900-MHz measured and modeled vertically polarized power-delay profiles for a vehicle outside the line-of-sight path as a distinct reflector. The model correctly predicted the amplitudes and arrival times of almost all significant multipath components in this complicated environment. The measured and simulated rms delay spreads were 96.86 and 63.7 ns, respectively. Similarly, the comparison of the measured and simulated power-delay profiles for 1800-MHz vertical polarization is depicted in Fig. 11(b). In this case, the vehicle was moving while the data were taken. Consequently, the arrival times of vehicle-caused multipath components were changed and the rms delay spread was greater.

V. Conclusion

A theoretical model based on the UTD for an impedance wedge was developed to study ultrahigh frequency (UHF) radio-wave propagation in tunnel environments. Theoretical prediction was compared to both narrow-band and wide-band measurements. For propagation in empty straight tunnel environments, both measurements and simulations indicated the existence of a distinct break point before and after which propagation exhibited different attenuation rates. Moreover, propagation in such idealized environments had very short delay spread and, thus, inherited a broad coherent bandwidth. In curved or branched tunnels, propagation suffered a larger loss which severely limited the coverage. Transmission and reception between the outside and inside of tunnels were hampered. Obstacles such as vehicles in tunnel environments made propagation even more complicated. The presence of a vehicle caused the received signal exhibit more severe fluctuations, large varying rms delay spreads, and additional loss. Previous works in tunnel propagation have focused on the frequency characteristics of narrow-band transmission and has not investigated the frequency characteristics of wide-band propagation. Our measurements and simulation revealed that higher frequency caused longer rms delay spreads, thus having a narrow coherent channel bandwidth. Such also concurs with the simulated narrow-band results in actual tunnel environments. The amplitudes and arrival times of individual multipath components in the wide-band system were accurately predicted; the calculated and measured rms delay spreads were found to be quite similar in most cases.

Appendix

The terms in (1) are explained as follows:

- R_{ik_r} reflection coefficient of the ith ray undergone k_r times specular reflections from corresponding reflected surfaces and then intercepted by the receive antenna;
- G_{ti} the square root of the gain of the transmit antenna in the direction of its launched ith ray;
- G_{ri} the square root of the gain of the receive antenna in the direction of its received ith ray;
- S_i spreading factor for the ith reflected ray;
- Φ_i phase factor for the ith reflected ray;
- $R_{uk_{rb}}$ reflection coefficient of the uth ray undergone k_{rb} times specular reflections from the corresponding reflected surfaces before being diffracted by wedge w and then intercepted by the receive antenna;
- D_{wu} diffraction coefficient of the uth ray at wedge w;
- $R_{uk_{rb}}$ reflection coefficient of the uth ray undergone k_{ra} times specular reflections from the corresponding reflected surfaces after being diffracted by wedge w and then intercepted by the receive antenna;
- G_{tu} the square root of the gain of the transmit antenna in the direction of its launched uth ray;
- G_{ru} the square root of the gain of the receive antenna in the direction of its received uth ray;
- S_u spreading factor for the uth ray involved with single diffraction at wedge w;
- Φ_u phase factor for the uth ray involved with single diffraction at wedge w;

$R_{vk_{rc}}$ reflection coefficient of the vth ray undergone k_{rc} times specular reflections from the reflected surfaces before being doubly diffracted by any two successive significant wedges and then intercepted by the receive antenna;

D_{wv} diffraction coefficient of the vth ray at wedge w;

D_{wv+1} second diffraction coefficient of the vth ray at the successive significant wedge;

$R_{vk_{rd}}$ reflection coefficient of the vth ray undergone k_{rd} times specular reflections from the corresponding reflected surfaces after being doubly diffracted by any two successive significant wedges and then intercepted by the receive antenna;

G_{tv} the square root of the gain of the transmit antenna in the direction of its launched vth ray;

G_{rv} the square root of the gain of the receive antenna in the direction of its received vth ray;

S_v spreading factor for the vth ray involved with double diffraction at any two successive significant wedges;

Φ_v phase factor for the vth ray involved with any two successive significant wedges.

$$R_h(\varphi,\varepsilon)=\frac{\mathrm{Sin}(\varphi)-\sqrt{\varepsilon-\mathrm{Cos}^2(\varphi)}}{\mathrm{Sin}(\varphi)+\sqrt{\varepsilon-\mathrm{Cos}^2(\varphi)}} \tag{A.1}$$

is the reflection coefficient for a ray reflected once from a reflected surface, and this ray is horizontally polarized with respect to the surface

$$R_v(\varphi,\varepsilon)=\frac{\varepsilon\,\mathrm{Sin}(\varphi)-\sqrt{\varepsilon-\mathrm{Cos}^2(\varphi)}}{\varepsilon\,\mathrm{Sin}(\varphi)+\sqrt{\varepsilon-\mathrm{Cos}^2(\varphi)}} \tag{A.2}$$

is the reflection coefficient for a ray reflected once from a reflected surface and this ray is vertically polarized with respect to the surface. All reflection coefficients in (1) have the form of $R_h(\varphi,\varepsilon)$ and $R_v(\varphi,\varepsilon)$ in which φ represents a reflection angle with respect to the local ray-coordinated system and $\varepsilon=\varepsilon_r-j60\sigma\lambda$

$$S_i=\frac{1}{L_i} \tag{A.3}$$

is the spreading factor for a reflected ray with propagation path length L_i

$$\Phi_i=\exp\left(-j\frac{2\pi L_i}{\lambda}\right) \tag{A.4}$$

is the phase factor for a reflected ray with propagation path length L_i.

The diffraction coefficients are given in (37) in Part 1 in which

$$\xi_1=\xi_2=\frac{-jk}{\sqrt{\varepsilon_r-j60\lambda\sigma}} \tag{A.5}$$

for an incident vertically polarized wave or

$$\xi_1=\xi_2=-jk\sqrt{\varepsilon_r-j60\lambda\sigma} \tag{A.6}$$

for an incident horizontally polarized wave

$$S_u=\frac{1}{L_{ub}}\left(\sqrt{\frac{s'_u}{s_u(s_u+s'_u)}}\right)\frac{1}{L_{ua}} \tag{A.7}$$

is the spreading factor for the uth ray involved with single diffraction at wedge w. S'_u is the distance of the diffraction or the reflection point to the source, and S_u, the distance of the diffraction or the reflection point to the observation. L_{ub} and L_{ua} are the path lengths of the uth ray before and after the diffraction point, respectively

$$\Phi_u=\exp\left(\frac{-j2\pi}{\lambda}(L_{ub}+s_u+s'_u+L_{ua})\right) \tag{A.8}$$

is the phase factor for the uth ray

$$S_v=\frac{1}{L_{vb}}\left(\sqrt{\frac{1}{s_{v1}s_{v3}(s_{v1}+s_{v2})(s_{v2}+s_{v3})}}\right)\frac{1}{L_{va}} \tag{A.9}$$

is the spreading factor for the vth ray involved with double diffraction. L_{ub} and L_{ua} are the path lengths of the vth ray before and after the wedge w

$$\Phi_v=\exp\left(\frac{-j2\pi}{\lambda}(L_{ub}+s_{v1}+s_{v2}+s_{v3}+L_{ua})\right) \tag{A.10}$$

is the phase factor for the vth ray.

A half-wavelength standard dipole was used for both transmit and receive antennas in the simulation. The gain of the antenna is

$$1.64\left[\frac{\mathrm{Cos}\left(\frac{\pi}{2}\mathrm{Cos}\,\theta\right)}{\mathrm{Sin}\,\theta}\right]^2 \tag{A.11}$$

where θ is measured from the axis of the dipole.

ACKNOWLEDGMENT

The authors would like to thank Prof. J. H. Sheng, Prof. Gue Xin Zheng, D. Poon, and T. Lo for their assistance in the measurements.

REFERENCES

[1] J. D. Parsons, *The Mobile Radio Propagation Channel.* London, U.K.: Pentech, 1992.

[2] S. Mockford, "Narrowband characterization of UHF mobile radio channels in rural areas," Ph.D. dissertation, Dept. Elect. Eng. Electron., Univ. Liverpool, Liverpool, U.K., 1989.

[3] A. S. Bajwa and J. D. Parsons, "Small area characterization of UHF urban and suburban mobile radio propagation," *Proc. IEE*, vol. 129, pt. F, no. 2, pp. 102–109, Feb. 1982.

[4] D. C. Cox, R. R. Murray, and A. W. Norris, "800 MHz attenuation measured in and around suburban houses," *AT&T Tech. J.*, vol. 63, no. 4, pp. 921–954, 1984.

[5] S. T. S. Chia, R. Steele, E. Green, and A. Baran, "Propagation and bit error ratio measurements for a microcellular system," *J. IERE*, vol. 57, no. 6, pp. S255–S266, 1987 (supplement).

[6] A. J. Rustako, M. J. Owens, and R. S. Roman, "Radio propagation at microwave frequencies for line-of-sight microcellular mobile and personal communications," *IEEE Trans. Veh. Technol.*, vol. 40, pp. 203–210, Feb. 1991.

[7] R. J. C. Bultitude and G. K. Bedal, "Propagation characteristics on microcellular urban mobile radio channels at 910 MHz," *IEEE J. Select. Areas Commun.*, vol. 7, pp. 31–39, Jan. 1989.

[8] T. S. Rappaport, "Characterization of UHF multipath radio channels in factory buildings," *IEEE Trans. Antennas Propagat.*, vol. 37, pp. 1058–1069, Aug. 1989.

[9] S. Y. Seidel and T. S. Rappaport, "Site-specific propagation prediction for wireless in-building personal communication system design," *IEEE Trans. Veh. Technol.*, vol. 43, pp. 879–891, Nov. 1994.
[10] W. Honcharenko, H. L. Bertoni, and J. L. Dailing, "Mechanisms governing propagation between different floors in buildings," *IEEE Trans. Antennas Propagat.*, vol. 41, pp. 787–790, June 1993.
[11] D. O. Reudink, "Mobile radio propagation in tunnels," in *IEEE Veh. Technol. Group Conf.*, San Francisco, CA, Dec. 1968.
[12] L. Deryck, "Natural propagation of electromagnetic waves in tunnels," *IEEE Trans. Veh. Technol.*, vol. VT-27, pp. 145–150, Aug. 1978.
[13] A. G. Emslie, R. L. Lagace, and P. F. Strong, "Theory of the propagation of UHF radio waves in coal mine tunnels," *IEEE Trans. Antennas Propagat.*, vol. AP-23, pp. 192–205, Mar. 1975.
[14] J. Chiba, T. Inaba, Y. Kuwamoto, O. Banno, and R. Sato, "Radio communication in tunnels," *IEEE Trans. Microwave Theory Tech.*, vol. MTT-26, pp. 439–443, June 1978.
[15] Y. Yamaguchi, T. Abe, T. Sekiguchi, and J. Chiba, "Attenuation constants of UHF radio waves in arched tunnels," *IEEE Trans. Microwave Theory Tech.*, vol. MTT-33, pp. 714–718, Aug. 1985.
[16] S. F. Mahmoud and J. R. Wait, "Geometrical optical approach for electromagnetic wave propagation in rectangular mine tunnels," *Radio Sci.*, vol. 9, no. 12, pp. 1147–1158, Dec. 1974.
[17] W. D. Burnside and K. W. Burgener, "High frequency scattering by a thin lossless dielectric slab," *IEEE Trans. Antennas Propagat.*, vol. AP-31, pp. 104–110, Jan. 1983.
[18] Y. P. Zhang and Y. Hwang, "Characterization of UHF radio propagation channels in tunnel environments for microcellular and personal communications," submitted to *IEEE Trans. Veh. Technol.*, to be published.
[19] V. Erceg, A. J. Rustato, and R. S. Roman, "Diffraction around corners and its effects on the microcell coverage area in urban and suburban environments at 900 MHz, 2 GHz, and 6 GHz," *IEEE Trans. Veh. Technol.*, vol. 43, pp. 762–766, Aug. 1994.
[20] T. Kementschits, A. L. Scholtz, and E. Bonek, "Microwave measurements in scaled road tunnels modeling 900 MHz propagation," in *Proc. 43rd IEEE Veh. Technol. Conf.*, Secaucus, NJ, May 1993, pp. 70–72.
[21] T. S. Rappaport, S. Y. Seidel, and R. Singh, "900-MHz multipath propagation measurements for US digital cellular radiophone," *IEEE Trans. Veh. Technol.*, vol. 39, pp. 132–139, May 1990.
[22] P. Mariage, M. Lienard, and P. Degauque, "Theoretical and experimental approach of the propagation of high frequency waves in road tunnels," *IEEE Trans. Antennas Propagat.*, vol. 42, pp. 75–81, Jan. 1994.

Y. P. Zhang, for a photograph and biography, see this issue, p. 1336.

Y. Hwang, for a photograph and biography, see this issue, p. 1336.

Robert G. Kouyoumjian, for a photograph and biography, see p. 22 of the January 1996 issue of this TRANSACTIONS.